Experimental and Analytical Investigation of a Stainless Steel Anchorage for CFRP Prestressing Tendons

Adil Al-Mayah
Research Assistant
Department of Civil Engineering
University of Waterloo
Ontario, Canada

Khaled A. Soudki, Ph.D., P.E.
Associate Professor
Department of Civil Engineering
University of Waterloo
Ontario, Canada

Alan Plumtree, Ph.D., P.E.
Professor
Department of Mechanical Engineering
University of Waterloo
Ontario, Canada

This paper presents the results of laboratory testing and mathematical modeling which describe the performance of a stainless steel wedge anchorage system for Carbon Fiber Reinforced Polymer (CFRP) tendons under static loading conditions. It was found that as the presetting load increased, the displacement of the rod and sleeve decreased. A finite element model (FEM) consisting of three contact surfaces was applied to simulate the anchor components and successfully model the displacement of the rod. An analytical model based on thick cylinder analogy was used to verify the contact pressure on the CFRP rod determined by FEM. A parametric study was conducted using FEM to investigate the effects of varying the presetting load and coefficient of friction between the anchor components. It was found that the effect of the coefficient of friction at the wedge barrel surface was minimal in comparison to the effect of the presetting load and coefficient of friction between the rod and sleeve.

Prestressing concrete with Fiber Reinforced Polymer (FRP) tendons is increasing in popularity because these composites have many attractive features compared to prestressing steel. Their high strength-to-weight and stiffness-to-weight ratios, as well as corrosion resistance, are extremely attractive properties which structural designers can exploit, in much the same way as aerospace engineers applied FRP materials 20 years ago.

The use of these materials allows the design of new structures as well as the rehabilitation or strengthening of structures with post-tensioning by using FRP rod-anchor systems. Oftentimes, repairs with prestressing steel are susceptible to corrosion and environmental changes not experienced by FRP.

Anchorage Systems

A problem facing the use of FRP in prestressing applications is their anchorage.[1] Different types of anchors have been used with FRP tendons, such as a clamp,[2,3,4] plug and cone,[5] resin sleeve,[3,6] potted resin,[7] expansive cement,[8] metal overlay,[1] and split wedge.[5,9,8,10]

Split wedge anchors which do not use resins are preferred because of their compactness, ease of assembly, reusability and reliability. These may consist of two, four or six wedges inserted into a barrel. Split wedge anchors are similar to those used for steel strands but are longer and have a soft metal sleeve encapsulating the rod to prevent notching.

Unfortunately, the anchors that are commercially available today are made of plain carbon steel which can be susceptible to corrosion.

The failure modes that have been observed using wedge anchors and FRP rods fall into two main categories:

The first is failure of the anchor system, including slip of the rod out of the anchor, slip of the sleeve and rod relative to wedges, slip of the wedges relative to the barrel, and rupture of the rod inside the anchor.

The second category is failure of the rod outside the anchor, thereby not involving the anchor.

To improve the performance of the anchor system, Shrive et al.[11] at the University of Calgary, as part of the ISIS Canada Programme, introduced a corrosion-resistant stainless steel anchorage system designed for 8 mm (5/16 in.), 104 kN (23.4 kips) specified tensile strength, Leadline™ CFRP tendons manufactured by Mitsubishi.[12]

In an attempt to improve the performance of the stainless steel anchor system, several developmental stages were undertaken.

To improve anchor grippage, different interference angles between the

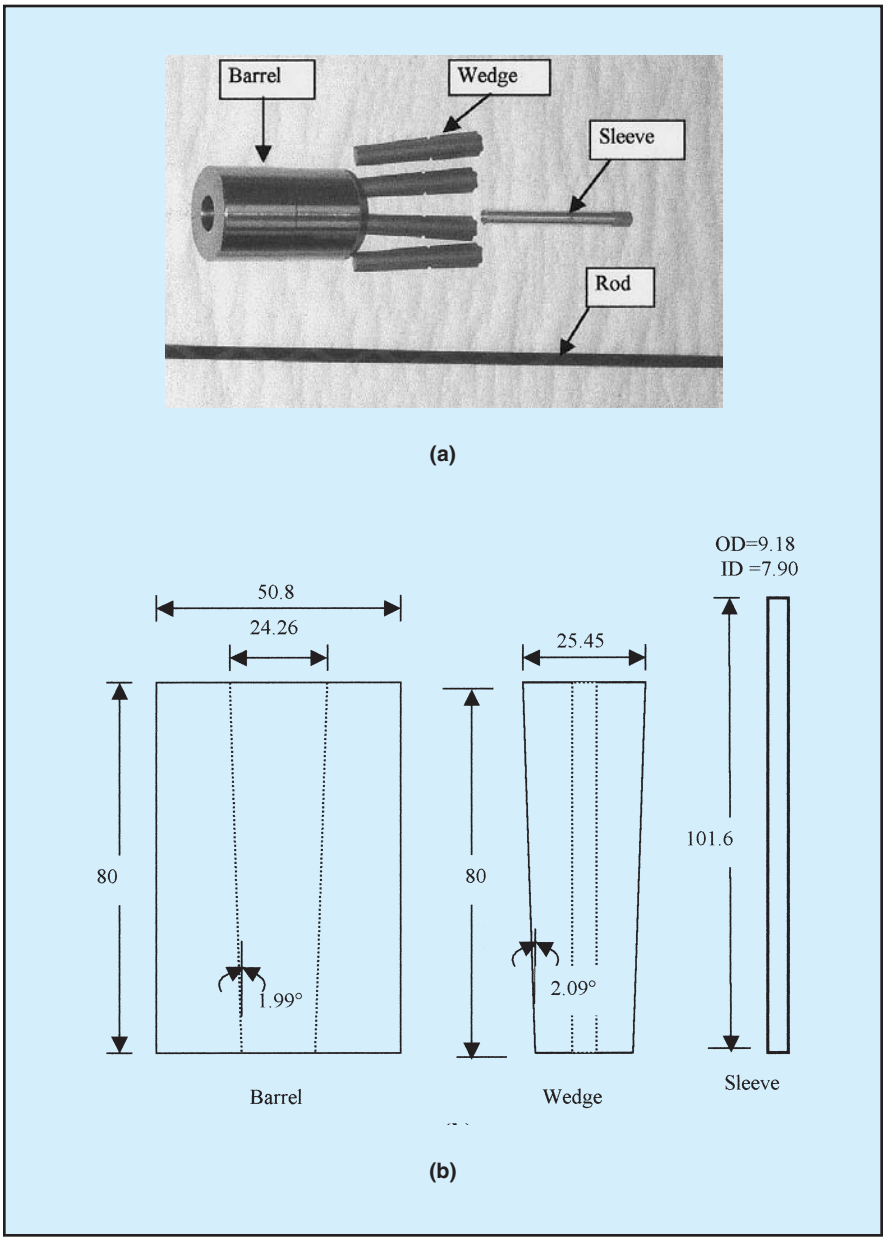

Fig. 1. Components of anchorage system: (a) Photographic; (b) Schematic.
Note: dimensions in mm; 1 in. = 25.4 mm.

Table 1. Mechanical properties of anchor components.

Property (1) Material	Rod (2) CFRP	Sleeve (3) Aluminum	Wedge (4) Stainless steel	Barrel (5) Stainless steel
Elastic modulus				
-Longitudinal direction, GPa	147	68.9	200	200
-Transverse direction, GPa	10.3	68.9	200	200
Shear modulus				
-Longitudinal direction, GPa	7.2	26	77	77
-Transverse direction, GPa	7.2	26	77	77
Major Poisson's ratio	0.27	0.35	0.33	0.33
Minor Poisson's ratio	0.02	0.35	0.33	0.33

Note: 1 in. = 25.4 mm, 1 kip = 4.448 kN.

contact surfaces at the inner face of the barrel and the wedges were tested. A sandblasted copper sleeve of 0.48 mm (0.019 in.) thickness was also used.

The main purpose of this soft metal sleeve was to produce a larger contact surface and to minimize stress concentrations between the tendon and the wedges. Further details of the wedge-anchor system are presented elsewhere.[8]

The present work presents a further development of this system, including the results of laboratory testing and mathematical modeling. Although described later, it is important to note that following these developments, failure always occurred outside the anchor.

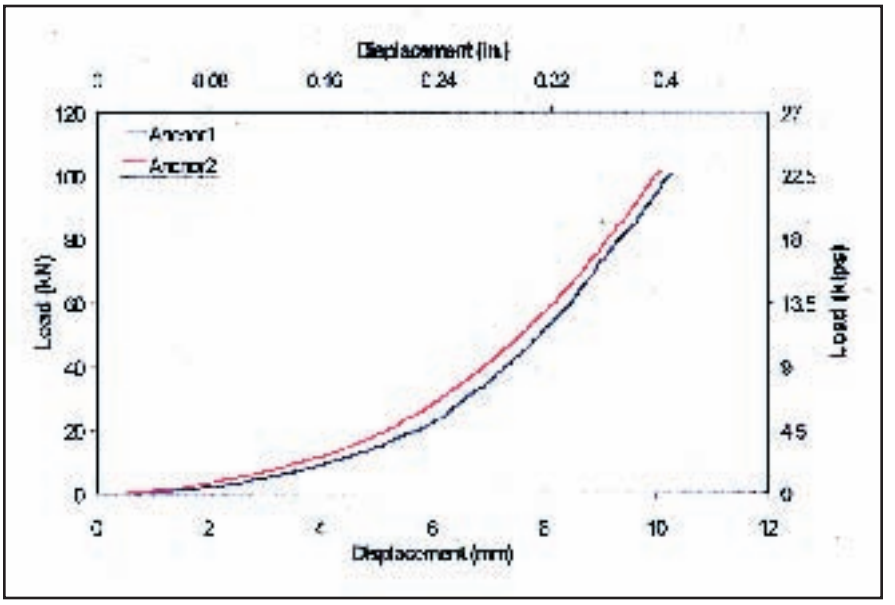

Fig. 2. Presetting load versus wedge displacement. Note: 1 in. = 25.4 mm, 1 kip = 4.448 kN.

Previous Experimental Studies

Most of the tests to date have concentrated on proof testing the rod-anchor system by determining its load capacity.

Nanni et al.[9] carried out static load tests to failure to determine the stress-strain relationship using Carbon Fiber Reinforced Polymer (CFRP), Glass Fiber Reinforced Polymer (GFRP), and Aramid Fiber Reinforced Polymer (AFRP) rods.

The CFRP-rod anchor system consisted of 8 mm (0.31 in.) diameter Leadline™ and a two-wedge anchor with a shredded aluminum sleeve made by Mitsubishi.[12] Although some slipping in the anchor components occurred, it was reported that the system was able to carry the fracture load of the rod.

Hodhod and Uomoto[10] conducted similar tests using two-wedge anchors with 6 mm (0.24 in.) diameter CFRP rods without a soft metal sleeve. The inner faces of the wedges were roughened by coating them with an adhesive and iron powder. Failure of the anchor system was caused by rupture of the rod due to non-uniform distribution of the radial stresses on the rod caused by the wedges.

Sayed-Ahmed et al.[8] conducted preliminary static tests on an anchor system similar to that used in the present study. The anchor comprised a copper sleeve, four stainless steel wedges and a stainless steel barrel. It was reported that the ultimate strength of the CFRP rod was achieved on loading.

Short-term sustained loading tests of different FRP rod-anchor systems were conducted by Nanni et al.[13] The tendons were stressed to 65 percent of their ultimate tensile strength for a three-day period, and load, strain and displacement readings were monitored during loading and under sustained load. For wedge anchor systems, steel wedges with or without a sleeve performed well in comparison to other wedge materials such as aluminum and plastic.

Cyclic, as well as static tests have been conducted by Grace and Sayed[14] on a highway bridge system. External post-tensioning was implemented using a Leadline™ CFRP rod anchor system supplied by Mitsubishi. No significant effect on the internal and external prestressing was reported.

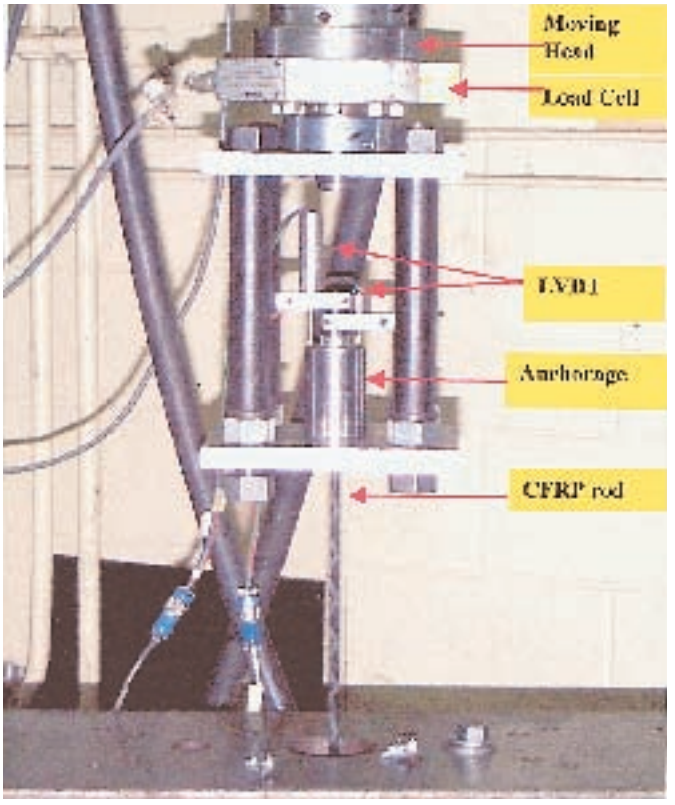

Fig. 3. Loading frame and test setup.

Sayed-Ahmed et al.[8] conducted satisfactory cyclic proof tests on the stainless steel anchor developed at the University of Calgary.

Previous Analytical Studies

Mitchell et al.[14] modeled an FRP rod-anchor system by using finite element analysis. The axisymmetric model consisted of an FRP rod bonded to the outer metal casing by a layer of potting material. Adhesive bonding occurred between the three parts of the anchor. The load was transferred from the FRP rod to the other parts by high shear stresses combined with relatively low normal stresses (shear fitting).

A parametric study was conducted to determine the effect of anchor length, modulus of elasticity of the potting material and its thickness at the inner end of the anchor, and the socket thickness. Strain of the rod within the anchor was measured for different parameters. The experimental and analytical results showed that the anchor was unable to carry the ultimate design load of the rod through lack of grip or rod failure.

The anchor system under consideration was modeled using finite elements by Sayed-Ahmed et al.[8] and Campbell et al.[15] Both models were essentially similar, with the wedge being isotropic in one[8] and orthotropic in the other.[15] However, the anchor was only partly modeled since the sleeve was not considered.

The radial and longitudinal stresses existing in the anchor, when the ultimate strength of the rod was attained, were the main concern in both investigations. The response of the anchor system with time was neglected.

Significance of Research

It is evident that more detailed attention must be directed towards examining the gripping mechanism of FRP-wedge anchor systems.

This research strives to provide a better understanding of the displacement behavior in a CFRP rod wedge-type anchor system under tensile load for different presetting loads.

In the analytical phase, the complete anchor system (rod, sleeve, wedge, and barrel) was modeled in order to study the mechanical behavior of the anchor loaded in a continuous manner until the ultimate load level of the rod was reached.[16]

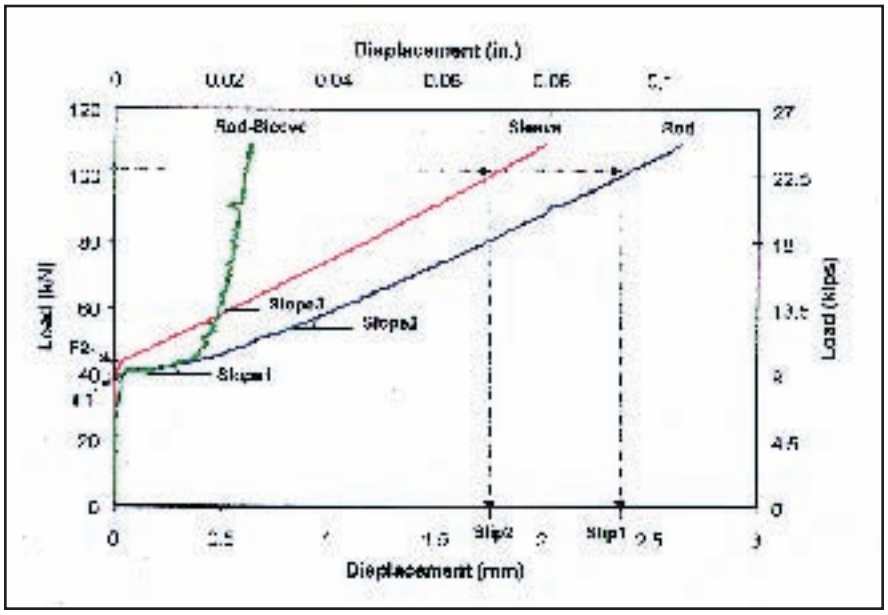

Fig. 4. Typical slip behavior of anchor components. Note: 1 in. = 25.4 mm, 1 kip = 4.448 kN.

The performance of the rod-anchor system was modeled using the finite element analytical technique. It is hoped that the results will provide a basis for future work in refining the anchor system.

Present Anchor System

Since inconsistent results were reported in the load-carrying capacity of the stainless steel anchor which used copper sleeves,[11] the present work attempted to increase the grip between the rod and sleeve by first inserting fine sand between the two components. However, no significant improvement was observed.

The focus then changed to substituting aluminum for the copper sleeve with varied sleeve thicknesses. It was found that a 0.64 mm (0.025 in.) thick aluminum sleeve gave optimum results. Failure of the rod consistently occurred outside the anchor. In all

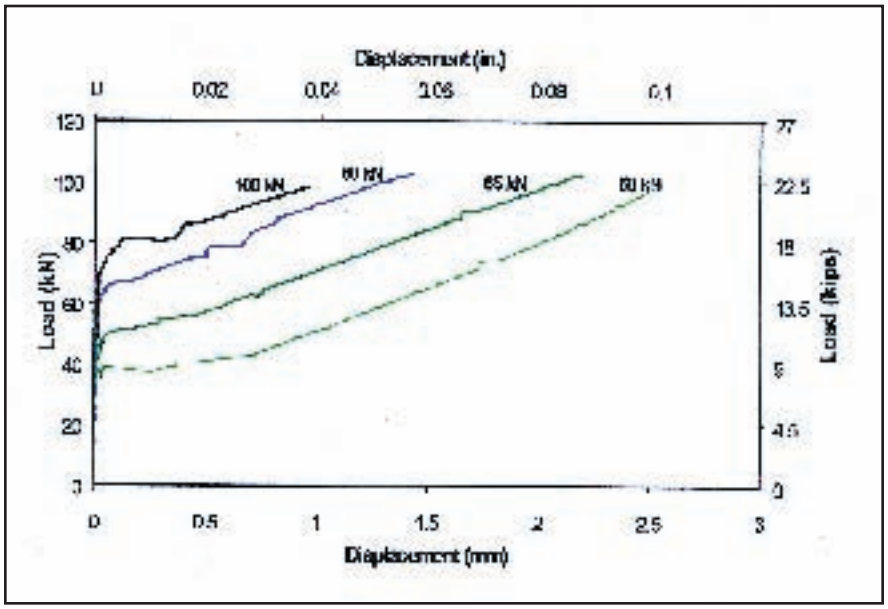

Fig. 5. Effect of presetting loads on rod displacement. Note: 1 in. = 25.4 mm, 1 kip = 4.448 kN.

cases, the maximum design load of the rod [104 kN (23.4 kips)] was achieved with minimum slip.

Fig. 1 shows this optimum design which consists of three components: a stainless-steel barrel with a conical socket; a four-piece stainless steel conical wedge set; and a thin aluminum sleeve placed between the wedges and the tendon. The mechanical properties of the different components are given in Table 1.[8]

The barrel was 50.8 mm (2 in.) in diameter and 80 mm (3.15 in.) long, while the larger diameter of the wedges was 25.45 mm (1.00 in.). The cone angle in the barrel was 1.99 degrees, 0.1 degree smaller than that of the wedges, so that as the wedges were inserted into the barrel, they gripped first on the tendon at the rear of the barrel. As the wedges seated further, they gripped the sleeve along their complete length. Since the soft metal sleeve was forced into the gaps between the wedges, there was a firm grip on the tendon.

LABORATORY TESTS

Details of the test specimen and experimental procedure are presented below and followed by the test results.

Test Specimen and Procedure

The test setup consisted of an anchor installed at each end of an 800 mm (31.50 in.) long CFRP Leadline™ rod. One of these was the wedge anchor (test anchor). Sixteen specimens were tested to investigate the behavior of the anchorage with aluminum sleeves under tensile load.

In order to establish a practical range for presetting load levels, four presetting loads were used: 50, 65, 80, and 100 kN (11.25, 14.61, 18.0, and 22.5 kips), respectively, representing 48, 63, 77 and 96 percent of the design load capacity of the tendon. Duplicate tests at each presetting load were carried out. At the other end, a reusable clamped anchor was used to grip the tendon.

A presetting rig consisted of a hydraulic jack attached to a steel frame. The jack assembly firmly installed the wedges into the barrel of the test anchor at the required load. Fig. 2 shows the presetting load versus displacement of the wedges relative to the barrel.

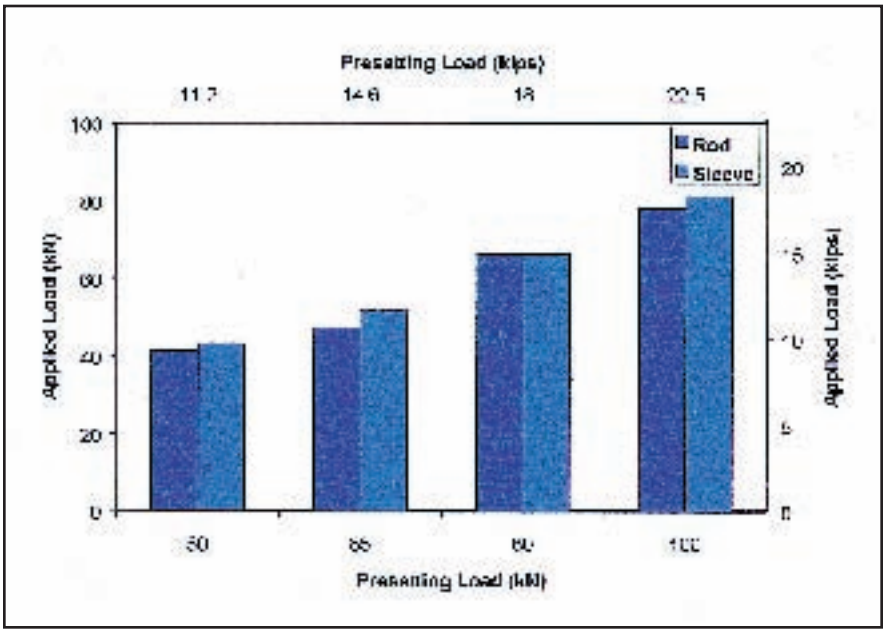

Fig. 6. Presetting load effect on slip initiation of the rod (F1) and sleeve (F2). Note: 1 in. = 25.4 mm, 1 kip = 4.448 kN.

The equipment used to test the anchor under static load was an electro-hydraulic servo-controlled universal testing machine, operated under displacement control. A load cell to monitor the force was attached to the bottom of the actuator.

Two Linear Variable Differential Transducers (LVDTs) measured the movement of the rod and sleeve relative to the barrel and their locations are shown in Fig. 3.

Test Results

Fig. 4 gives a typical load versus displacement plot for the rod and sleeve in the anchor. The rod displacement showed three distinct regions.

The first started when the load reached a threshold value of *F1*. Only the rod moved at a load-displacement rate, given by *Slope1*, until the applied load reached *F2*. At this point, the sleeve started to slip. The rate of load-displacement of the rod increased to *Slope2*. Note that the load continued to increase until the ultimate design tensile load of the rod was reached.

Fig. 4 shows that at 100 kN (22.5 kips), the rod had moved by an amount *Slip1* [2.37 mm (0.093 in.)] and the sleeve by *Slip2* [1.76 mm (0.069 in.)]. The sleeve load-displacement rate (*Slope3*) was greater than *Slope2*. During this stage, the sleeve and wedges were moving together.

Fig. 5 shows the effect of presetting load on rod displacement. Four different levels of presetting load of 50, 65, 80, and 100 kN (11.25, 14.61, 18.0, and 22.5 kips) were tested and the corresponding load versus rod displacement are illustrated in the figure.

As the presetting load increased, the rod displacement decreased significantly due to increased grip at the contact surface, which is a function of the contact area and pressure. By increasing the presetting load, the wedges were forced into a progressively smaller diameter, causing the contact pressure to increase.

The contact area of the wedge-barrel and rod-sleeve interfaces increased by increasing the presetting load due to a larger insert length of the wedges inside the barrel as shown in Fig 2. The contact surface between the sleeve and rod increased by plastically deforming the soft sleeve material and forcing it to flow into the spiral indentations of the rod.

Fig. 6 illustrates the effect of presetting load on the load levels at which the rod and sleeve displayed initial displacements (*F1* and *F2*, respectively). An increase in *F1* and *F2* was observed as the presetting load increased. By increasing the presetting load from 50 to 100 kN (11.16 to 22.5

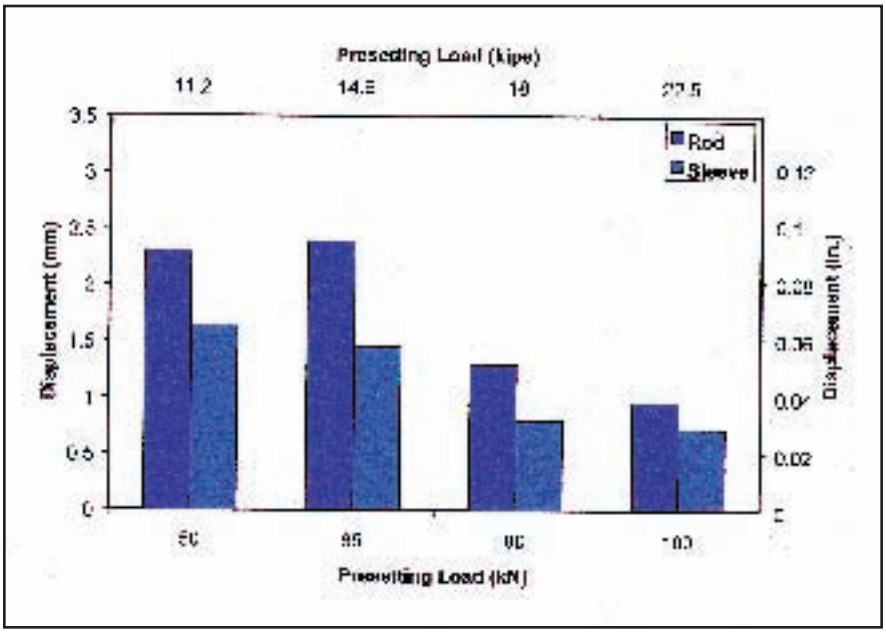

Fig 7. Presetting load effect on displacement of rod (*Slip1*) and sleeve (*Slip2*) at 100 kN applied load. Note: 1 in. = 25.4 mm, 1 kip = 4.448 kN.

kips), the threshold load of the rod (*F1*) increased by 37 kN (8.32 kips).

A similar response for the threshold for sleeve movement is shown in Fig. 6. As the presetting load increased from 50 to 100 kN (11.16 to 22.5 kips), the threshold (*F2*) increased by 38 kN (8.55 kips).

The effect of presetting load on the rod displacement at an applied load of 100 kN (22.5 kips) is shown in Fig. 7. When the presetting load increased from 50 to 100 kN (11.25 to 22.5 kips), the rod displacement (*Slip1*) decreased by 1.3 mm (0.051 in.) and the displacement of the sleeve (*Slip2*) decreased by 0.9 mm (0.035 in.).

This is a general effect. Fig. 4 shows that the load required to displace the rod at the first stage of slip was less than that required to move the rod and sleeve together. Also, the sleeve required a higher load than that of the rod to move one unit length.

Fig. 8 shows the slipping rates of the rod (*Slope1*, *Slope2*) and sleeve (*Slope3*) for different presetting loads. Constant values of 13 and 18 kN/mm (74 and 103 kips/in.) were found for *Slope1* and *Slope2*, respectively, for any presetting load.

However, this is not the case for *Slope3*. As the presetting load increased, the rate of slip of the sleeve (*Slope3*) increased. In other words, the load required to displace the sleeve one unit length was higher for large presetting loads than that for lower presetting levels.

FINITE ELEMENT MODEL

This section considers the finite element model configuration and results relative to the radial and longitudinal stress distributions. The results are compared to the experimental data.

Model Configuration

In general, there are three types of contact elements in finite element modeling: gap, slide line, and general elements.

Gap elements are suitable in finite sliding simulations because the main requirement is alignment between the elements of the two contacting bodies.

Slide line contact elements are usually used in simulating large amounts of slip.

General contact elements used in this study are the simplest. While they provide the most realistic contact pressure distribution, they are also the most intensive to compute.

A total of 355 axisymmetric linear quadratic elements were employed to model the anchor using an ABAQUS finite element package.

Three contact surfaces were included to simulate the interaction between any two adjacent parts. Each surface possessed a corresponding coefficient of friction based on the best description of the experimental data given in Fig. 5.

The coefficient of friction between rod and sleeve varied in a linear manner from 0.16 for the first loading step to 0.3 for the last step. The coefficient of friction of the wedge-barrel interface was given a constant value of

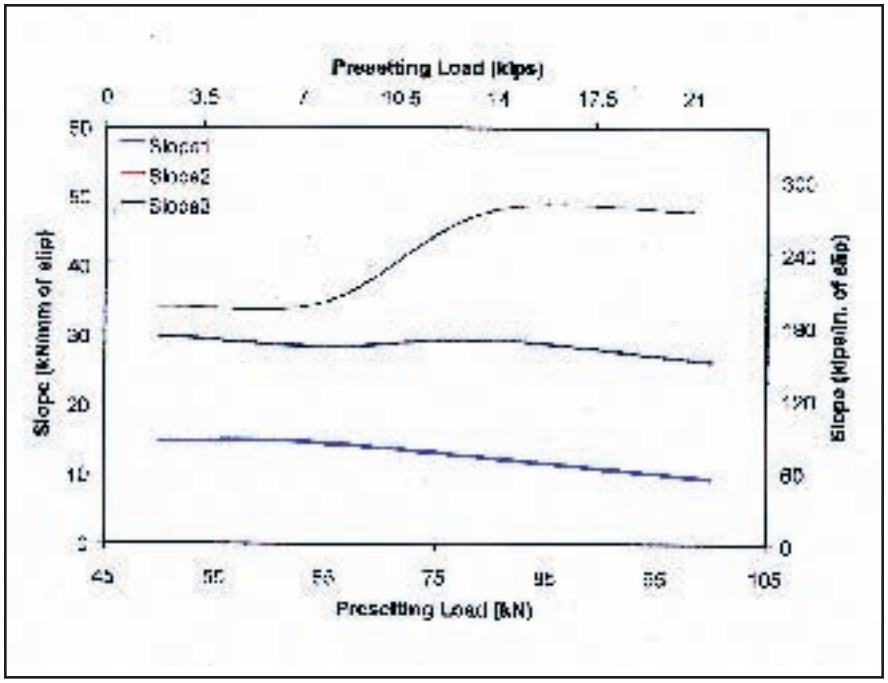

Fig 8. Presetting load effect on displacement rate of rod *Slope1, Slope2,* and sleeve *Slope3.* Note: 1 in. = 25.4 mm, 1 kip = 4.448 kN.

0.07 due to the nature of the bodies forming this surface.

The experimental results showed that the sleeve and wedge moved in unison. Consequently, the coefficient of friction at their interface was high, and defined as a rough surface in accordance with the ABAQUS program.

The boundary conditions during loading were either constant or variable. Note that the constant boundary conditions included preventing the rod from moving in a radial direction by confining its movement to take place in the longitudinal direction. Conversely, the barrel was prevented from moving in the longitudinal direction (see Fig. 9a).

The variable boundary conditions simulated the loading stages: first, by presetting while inserting the wedges into the barrel (see Fig. 9b); and then, by tensile loading of the rod (see Fig. 9c).

Only one loading step was used in the presetting process whereas 15 steps were used to simulate tensile loading. The presetting load was developed through displacement of the wedges in accordance with the experimental data taken during the anchor set tests presented earlier (see Fig. 2).

Once the rod, sleeve, and wedges had been forced into the barrel, the presetting load was released, leaving them under pressure. Tensile loading was then simulated by progressively pulling on the rod. The rate of loading was 0.25 mm (0.01 in.) for each of the 15 steps until the ultimate design load (104 kN) of the rod was reached.

Radial Stress Distribution

It is well known that CFRP is orthotropic and weak in the transverse direction. Thus, the radial stress should be at its lowest value in the region of high longitudinal stress to prevent undesirable stress concentrations from developing.

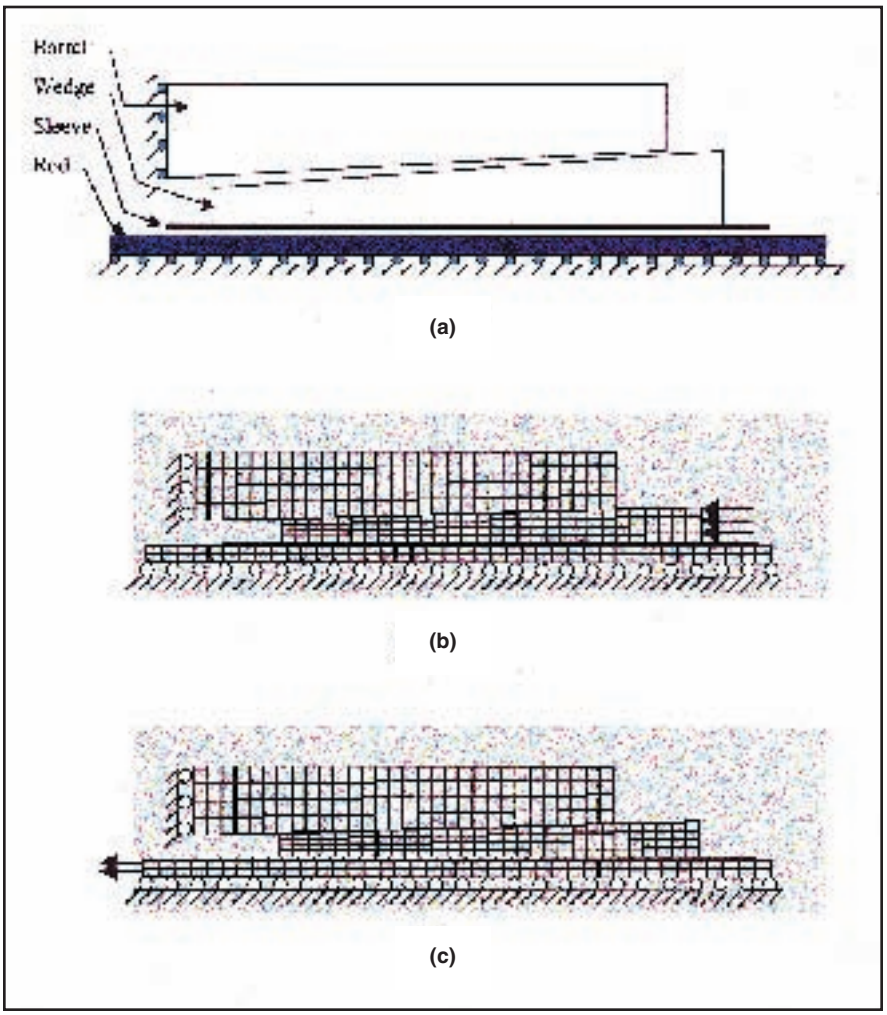

Fig. 9. Finite element model: (a) Geometry; (b) Presetting process; (c) Tensile loading.

The distribution of the radial stress for different presetting displacements with coefficients of friction of 0.07 and 0.16 at wedge-barrel, and rod-sleeve surfaces, respectively, are shown in Figs. 10(a) and (b). Again, these values were chosen based on the best description of the experimental results.

Figs. 10(a) and (b) illustrate that a high radial pressure was setup in the region where the wedges entered the barrel. Before applying the presetting load, there was only one location where the wedges were in contact with the barrel due to the interference fit.

The increase in the presetting load increased the contact area between the wedges and barrel. This resulted in a higher radial pressure at the first contact point and a lower radial pressure at the far end of the anchor.

The radial pressure decreased towards the core of the anchor where the rod was located, indicating that the radius of the wedges contributed effectively in transferring the radial pressure of the rod.

The most affected region was where the wedges entered the barrel, thus explaining the indentations at the surfaces of the wedges and the barrel, as observed after testing.

Longitudinal Stress Distribution

The distribution of the longitudinal stress along the rod is an important factor and is shown in Figs. 11(a) and (b) for an insert distance of 8.5 mm (0.33 in.), which corresponds to a presetting load of 65 kN (14.61 kips). In this case, the coefficient of friction of 0.16 at the rod-sleeve interface increased by 0.015 in each of the 15 loading steps.

The highest stress level occurred at the point where the rod entered the anchor and corresponded to expected locations where the stress was concentrated. The stress decreased in the rod as the distance increased from the loaded end.

The longitudinal stress decreased with increased shear stress that was generated by a gradual increase in the coefficient of friction and normal stress.

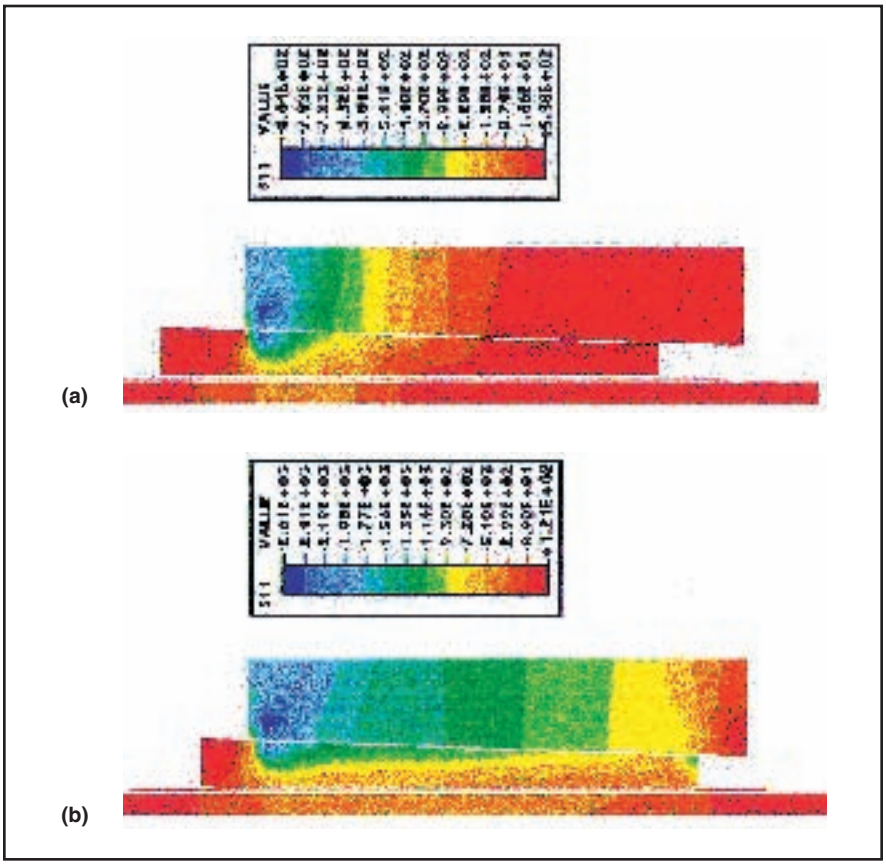

Fig. 10. Radial stress distribution (MPa) with presetting distance of (a) 3 mm and (b) 9 mm. Note: 1 in. = 25.4 mm, 1 kip = 4.448 kN.

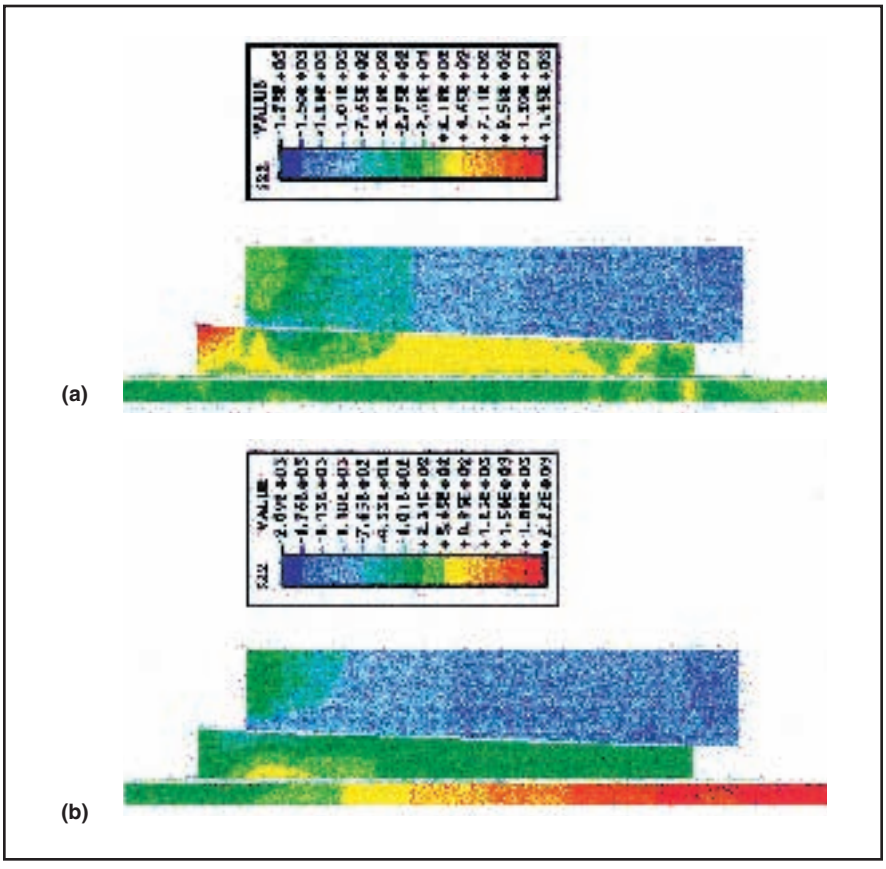

Fig. 11. Longitudinal stress distribution (MPa) with rod tensile load of (a) 0.0 and (b) 2.75 mm. Note: 1 in. = 25.4 mm, 1 kip = 4.448 kN.

Comparison of FEM and Experimental Results

In Fig. 12(a), the experimentally measured rod displacement for a presetting load of 65 kN (14.61 kips) is compared to the FEM description.

For this presetting load, the equivalent insert distance of the wedges in the barrel was 8.5 mm (0.33 in.). The coefficient of friction between the rod and sleeve varied from 0.16 for the first loading step to 0.3 for the last loading step, as mentioned earlier.

Also, the coefficient of friction between the wedges and the barrel was 0.07 which remained unchanged during the loading process. It is apparent from Fig. 12(a), that there is very good correlation between the experimental and numerical results.

Fig. 12(b) shows the slip of the rod using a higher presetting load of 100 kN (22.5 kips) caused by 10 mm (0.39 in.) insert distance while keeping the coefficients of friction the same as those used for the presetting load of 65 kN (14.61 kips) above.

The numerical curve remained consistently below the experimental plot, underestimating the load for a given displacement. However, the discrepancy was within 10 percent at most, indicating a reasonable agreement, although not as good as that for the lower presetting load.

It is possible that the coefficient of friction at the various presetting load levels increased because the amount of deformation of the contacting bodies increased with presetting load. As the applied normal pressure on these bodies increased, the amount of grip increased accordingly due to an increase in the actual area of contact.

PARAMETRIC STUDY USING FEM

The parameters studied include presetting load, coefficient of friction between the wedges and barrel, as well as that between the rod and sleeve and their effect on slippage of the rod.

Presetting Load

It was shown experimentally that the displacement of the rod decreased as the presetting load increased due to higher contact pressures on the sur-

faces. Increasing the contact pressure led to an increase in contact shear for a given coefficient of friction, resulting in less slip.

Fig. 13 shows the tensile load versus displacement of the rod for different presetting distances of 7.85, 8.5, 9 and 10 mm (0.31, 0.33, 0.35 and 0.39 in.), representing presetting loads of 50, 65, 80, and 100 kN (11.25, 14.61, 18.0, and 22.5 kips). As the presetting distance increased, the load versus displacement curve shifted upwards. This resulted in less slip when the ultimate design load (104 kN) of the rod was reached.

Note that the slopes of the curves, as well as the initiation loads for slip, were similar to the experimental results, i.e., increasing the presetting load decreased the sliding distance. For presetting distances of 7.85 mm and 9 mm (0.31 and 0.35 in.), numerical instability occurred in the analysis before the load level of the other presetting distances was reached. This caused non-convergence in the model. That is why dotted trend lines are shown in Fig.13.

Coefficient of Friction Between Wedges and Barrel

The effect of varying the wedge-barrel coefficient of friction between 0.03 and 0.13 while fixing the presetting distance at 8.5 mm or 0.33 in. (65 kN or 14.61 kips) and maintaining the range for the rod-sleeve coefficient of friction at 0.16 to 0.3, is shown in Fig. 14. As the coefficient of friction increased, the load versus displacement curve shifted down slightly.

This effect is considered less significant than that of presetting load. The slight differences in displacement due to the effect of different coefficients of friction resulted from inserting the wedges at different lengths into the barrel during the loading stage. For a lower coefficient of friction, less shear occurred, which resulted in a slightly larger displacement for a given tensile load.

Coefficient of Friction Between Rod and Sleeve

Due to deformation of the rod and particularly the sleeve, the coefficient of friction was not constant during the

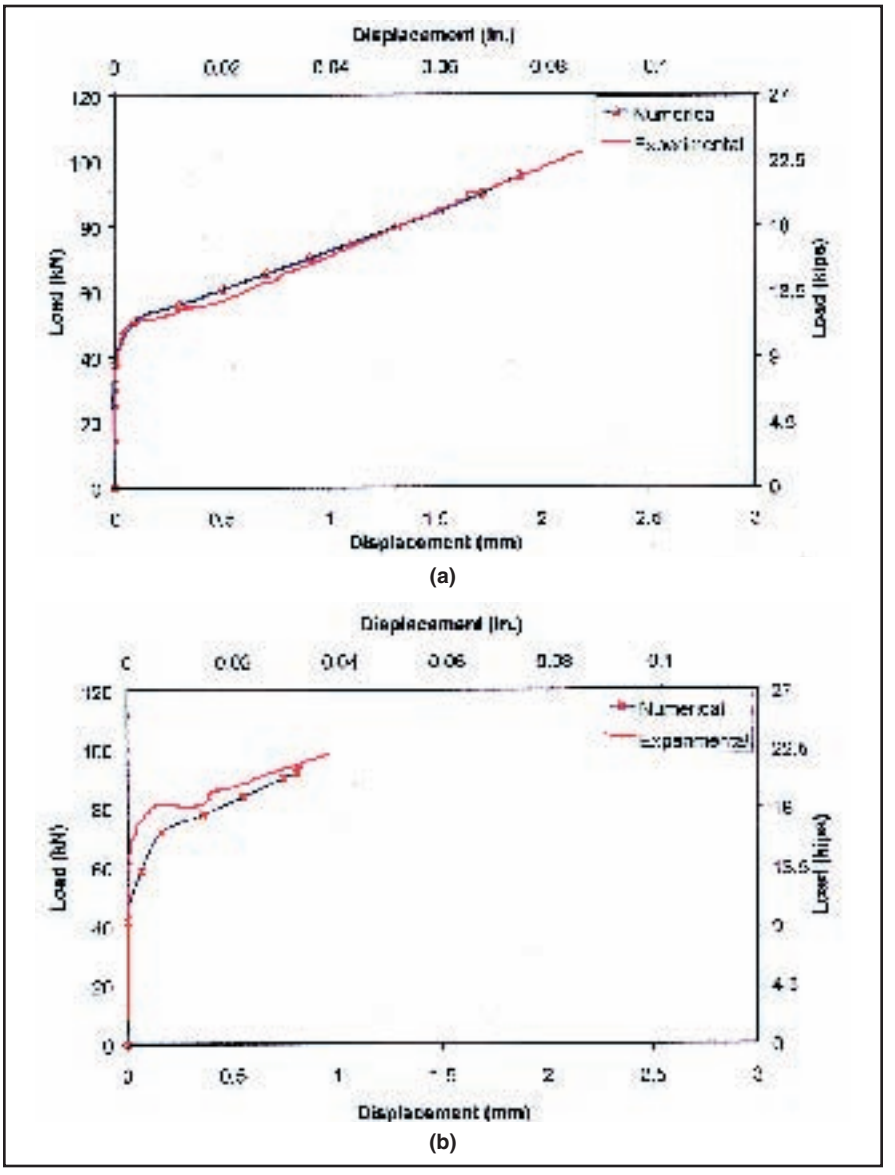

Fig. 12. Displacement of the rod with presetting load of (a) 65 kN and (b) 100 kN. Note: 1 in. = 25.4 mm, 1 kip = 4.448 kN.

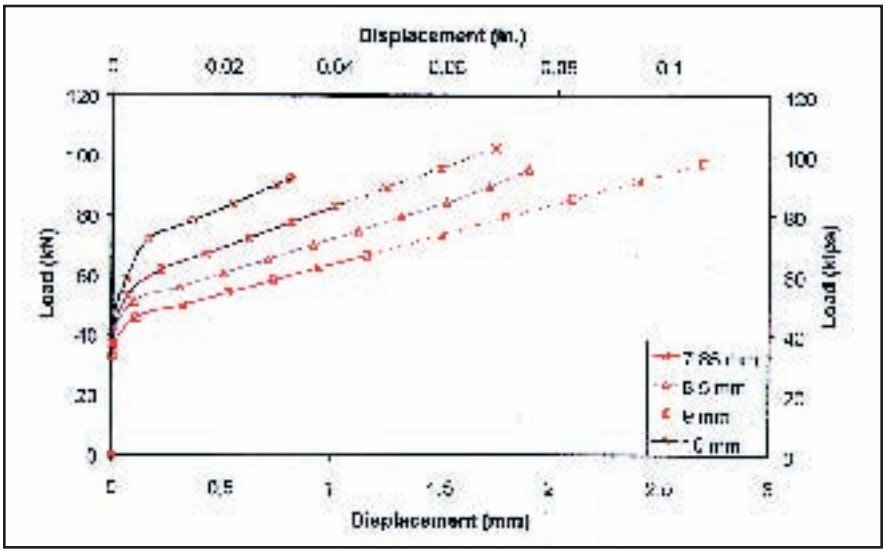

Fig. 13. Effect of presetting load on rod displacement Note: 1 in.= 25.4 mm, 1 kip= 4.448 kN.

various loading stages. Incremental changes of the coefficient of friction may vary from one step to another due to the interaction between the presetting distance and the contact pressure versus the coefficient of friction. However, this change was not large enough to affect the resistance of the rod to slip.

As mentioned earlier, the slipping resistance of the rod was generally a function of the normal stress and coefficient of friction. Increasing the coefficient of friction increased the shear resistance. Therefore, less rod displacement occurred as the applied tensile force and corresponding coefficient of friction at a particular contact surface increased, as shown in Fig. 15.

The values of the coefficient of friction were chosen to accurately describe the experimental values. Accordingly, the initial values for the coefficient of friction increased progressively in four instances, starting from 0.1, 0.16, 0.2 and 0.25, respectively, to a common final value of 0.3 at the end of the loading process. It is apparent that varying the friction at the rod-sleeve interface had a significant effect on the load-slip mechanism.

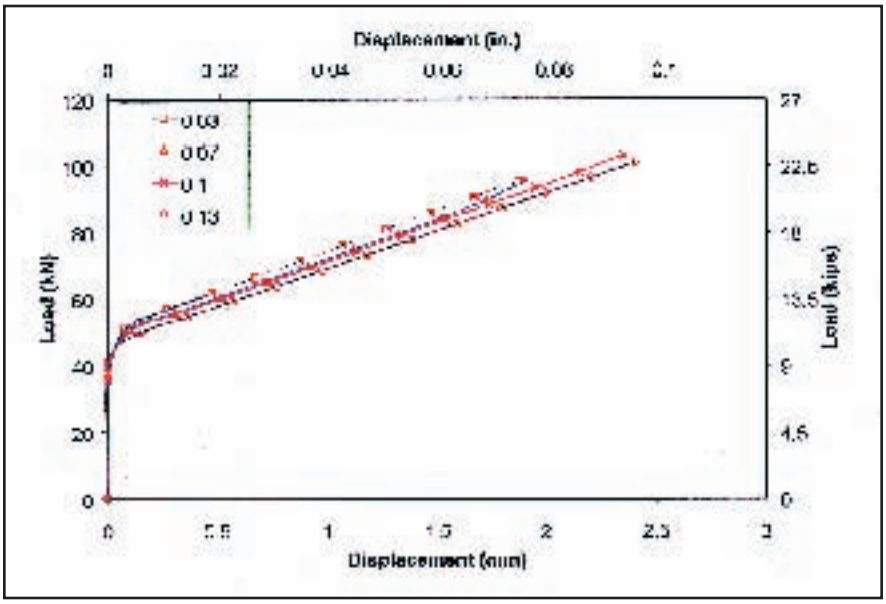

Fig. 14. Effect of coefficient of friction at wedge-barrel surface on rod displacement. Note: 1 in. = 25.4 mm, 1 kip = 4.448 kN.

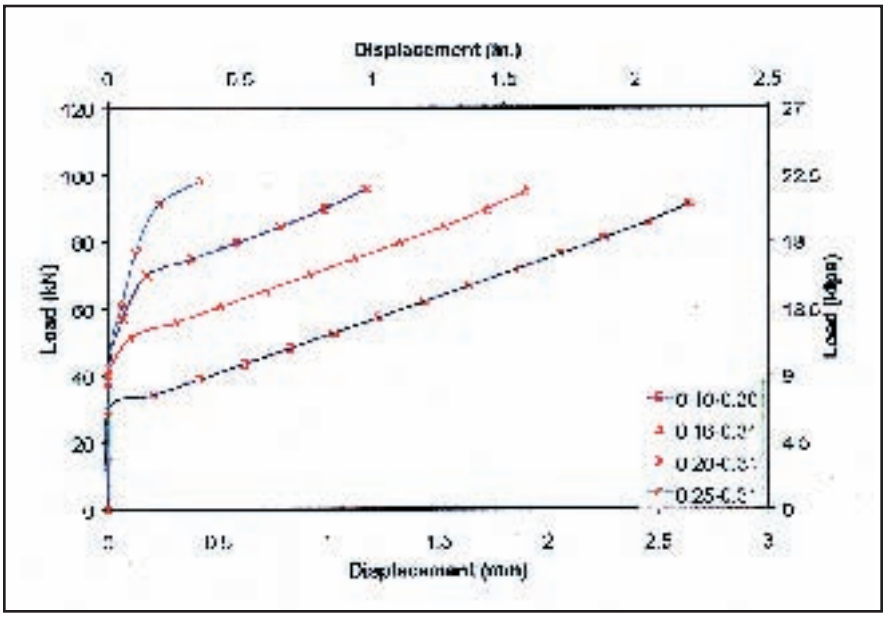

Fig. 15. Effect of coefficient of friction at rod-sleeve surface on rod displacement. Note: 1 in. = 25.4 mm, 1 kip = 4.448 kN.

ANALYTICAL MODEL

An analytical model based on the force fitting principle used in thick cylinder analysis was developed.

For a hollow cylinder with inner and outer diameters of (a) and (b), respectively, and subjected to an inner pressure of (p_i) and outer pressure (p_o), the radial displacement (u) at any distance (r) can be determined using the following equation proposed by Wang:[17]

$$Eu = \frac{p_i a^2 - p_o b^2}{b^2 - a^2}(1 - v)r - \frac{a^2 b^2 (p_o - p_i)}{b^2 - a^2}(1 + v)\frac{1}{r} \quad (1)$$

In order to apply Eq. (1) to determine the pressure on the particular surface, as well as to overcome the varied thicknesses of the wedges and barrel, the anchor was divided into nine sections along its length.

Each section is a disk consisting of four cylinders (CFRP rod as shaft, sleeve, wedges, and barrel) as shown in Fig. 16. The contact pressure is determined according to the radial displacements of each cylinder.

The radial displacement of each anchor component can be found using Eq. (1) as follows:

$$u_r = f(E_r, \nu_r, p_1, r) \quad \text{where } 0 \le r \le r_{or} \quad (2)$$

$$u_s = f(E_s, \nu_s, p_1, p_2, r) \quad \text{where } r_{is} \le r \le r_{os} \quad (3)$$

$$u_w = f(E_w, \nu_w, p_2, p_3, r) \quad \text{where } r_{iw} \le r \le r_{ow} \quad (4)$$

$$u_b = f(E_b, \nu_b, p_3, p_4, r) \quad \text{where } r_{ib} \le r \le r_{ob} \quad (5)$$

Four boundary conditions were applied to solve these displacement equations:

$$u_r (r = r_{or}) = u_s (r = r_{is}) \quad (6)$$

$$u_s (r = r_{os}) = u_w (r = r_{iw}) \quad (7)$$

$$u_w (r = r_{ow}) - u_b (r = r_{ib}) = \delta \quad (8)$$

$p_4 = 0$ in case of no constraint on outer face of barrel (9a)

or

$u_b\,(r = r_{ob}) = 0$ when outer face of barrel is constrained (9b)

The Maple V5 program was used to solve Eqs. (2) to (5), allowing the contact pressure on the various anchor components to be determined.

Comparison of Analytical and Finite Element Models

Figs. 17(a) and (b) compare the contact pressure distribution on the rod-sleeve interface for presetting inserts of 8.5 and 10 mm or 0.33 and 0.39 in. (65 and 100 kN or 14.61 and 22.5 kips) using the analytical and finite element models. It is apparent that the models give a similar variation of contact pressure along the anchor.

The contact pressure increased along the longitudinal axis, moving from the loaded end to the free end of the anchor. This was due to the 0.1 degree difference between the two tapers of the wedge and barrel.

At the loaded end of the anchor where the rod entered the anchor, the difference between the outer diameter of the wedges and the inner diameter of the barrel was at its lowest value. This was intended to avoid a high normal pressure in the region of high longitudinal tensile stress, thus avoiding stress concentrations. This can be seen in both the analytical and finite element models.

Nonetheless, there is a slight difference in values between the results of the analytical and numerical methods. The higher contact pressures given by the analytical method result from the use of elastic material properties in the theoretical model, upon which all of the equations were based; whereas plastic properties of the sleeve were used in the FEM.

The theoretical model was not only used to validate the FEM results. It also gave an efficient closed-form solution for the magnitude of the radial pressure between the CFRP rod and anchor system. This knowledge will assist the designer of an anchor in quantifying the pressure distribution

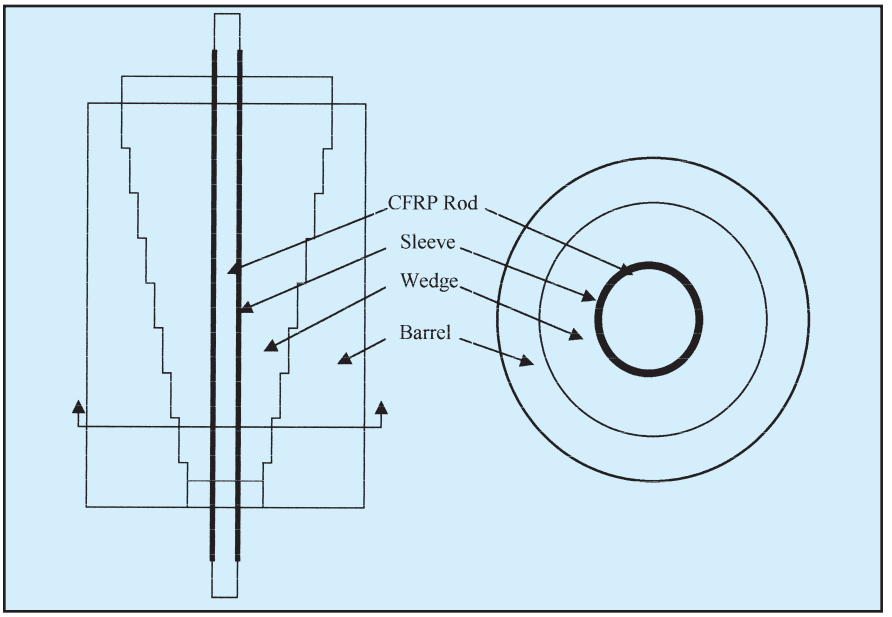

Fig 16. Analytical model.

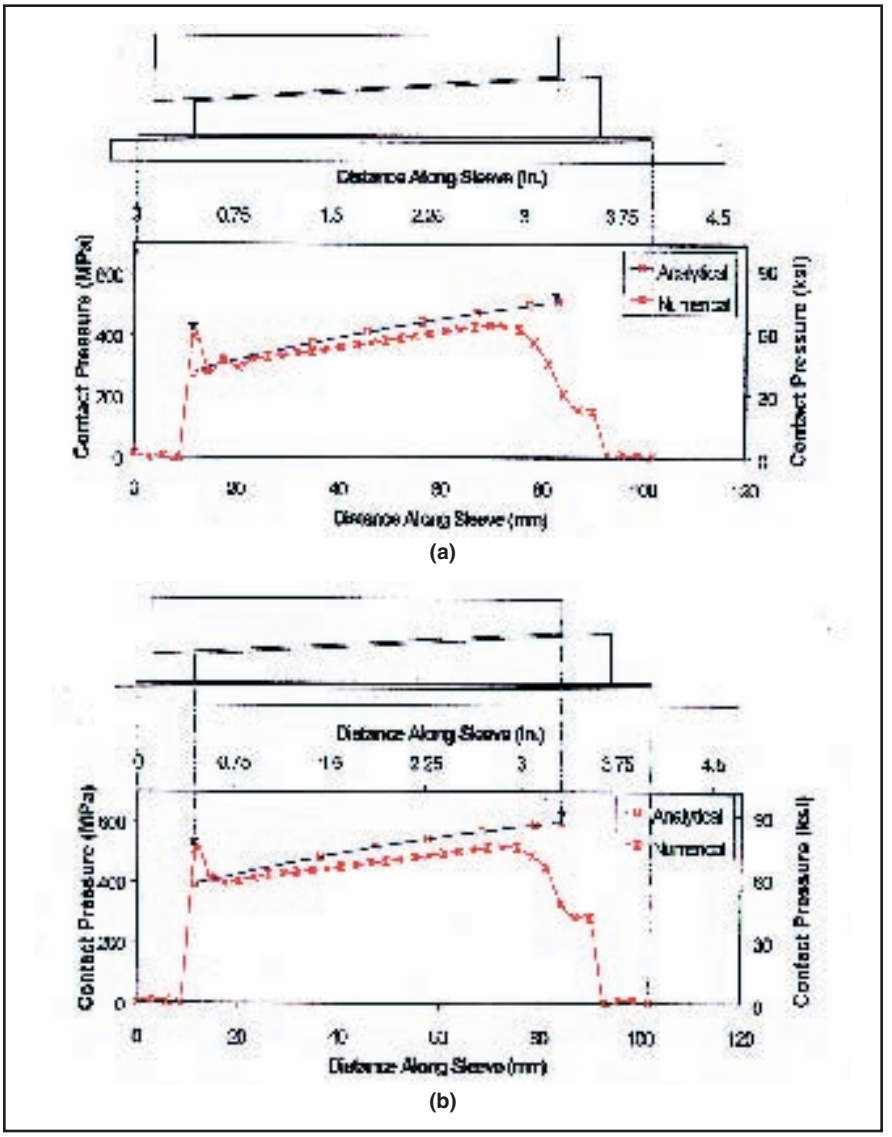

Fig. 17. Contact pressure on rod with presetting load of (a) 65 kN, (b) 100 kN. Note: 1 in. = 25.4 mm, 1 kip = 4.448 kN.

before a more detailed and time-consuming analysis is carried out.

CONCLUDING REMARKS

Based on the results of this investigation, the following conclusions can be drawn:

1. Using the four-wedge stainless steel anchor system modified by the authors, it is possible to prestress CFRP tendons up to their maximum acceptable design load without failure.

2. The test system allows the amount of slip in all anchor components, including the CFRP tendon, to be monitored for any given presetting load.

3. With progressively higher presetting loads, the amount of slip in the tendon and its sleeve decreased due to increased contact pressure and grip at the contact surfaces. Minimal slip occurred at the other interfaces. This behavior was modeled using finite element analysis, giving good agreement with the experimental data.

4. A parametric study showed a similar effect. The amount of slip in the tendon decreased with presetting load and increase in coefficient of friction between the tendon and sleeve, resulting from an increase in shear resistance at its interface.

5. By applying an analytical model using the thick cylinder approach, the contact pressures on the surfaces were determined and found to be in good agreement with the finite element analysis.

RECOMMENDATIONS

Use of FRP composites by the prestressed concrete industry in North America has been limited partly due to the lack of corrosion-resistant anchorage systems.

Physical testing and numerical modeling show that, based on the well-established prestressing technologies, a stainless steel wedge-type anchor can be used successfully with CFRP tendons. Such an anchor, unlike the steel strand anchor, requires preseating wedges to fully grip the CFRP tendon.

It is recommended that a presetting load in the range of 60 to 80 percent of the ultimate strength of the tendon be applied. This load should not be confused with the allowable stresses in the tendon which are typically 40 to 60 percent of their ultimate strength.

The tendon slip data presented in the paper allow quantification of the anchorage seating loss in post-tensioned prestressed concrete applications.

ACKNOWLEDGMENT

This work was supported by the University of Waterloo Interdisciplinary Grants Program.

Partial funding for the stainless steel anchors was provided by the Network of Centres of Excellence on Intelligent Sensing for Innovative Structures (ISIS Canada). This support is gratefully acknowledged.

The authors wish to express their gratitude to the PCI JOURNAL reviewers for their suggestions and constructive comments.

REFERENCES

1. Erki, M. A., and Rizkalla, S. H., "Anchorage for FRP Reinforcement," *Concrete International*, V. 15, No. 6, June 1993, pp. 54-59.
2. Malvar, L. J., and Bish, J., "Grip Effects in Tensile Testing of FRP Bars," *Non-Metallic (FRP) Reinforcement for Concrete Structures* (Edited by L. Taerwe), E & FN Spon, Chapman & Hall, London, United Kingdom, 1995, pp. 108-115.
3. Sippel, T. M., "Design, Testing, and Modelling of an Anchorage System for Resin Bonded Fibreglass Rods Used as Prestressing Tendons," *Advanced Composite Materials and Structures* (Edited by the Canadian Society for Civil Engineering), Montreal, Quebec, Canada, 1992, pp. 363-372.
4. Scheibe, M., and Rostasy, F. S., "Aspects of Laboratory Testing to Determine Mechanical Properties of FRP," *Non-Metallic (FRP) Reinforcement for Concrete Structures* (Edited by L. Taerwe), E & FN Spon, Chapman & Hall, London, United Kingdom, 1995, pp. 116-123.
5. Burgoyne, C. J., "Parafil Ropes for Prestressing Applications," *Fibre-Reinforced-Plastic (FRP) for Concrete Structures: Properties and Applications* (Edited by A. Nanni), Elsevier Science Publisher, New York, NY, 1993, pp. 333-351.
6. Reda, M. M., Sayed-Ahmed, E. Y., and Shrive, N. G., "Towards a New Non-Metallic Anchorage System for Post-Tensioned Applications with Carbon Fiber Reinforced Plastic Tendons," 42nd International SAMPE Symposium, 1994, pp. 288-297.
7. Holte, L. E., Dolan, C. W., and Schmdit, R. J., "Epoxy Socketed Anchors for Non-Metallic Prestressing Tendons," *Fibre-Reinforced-Plastic Reinforcement for Concrete Structures,* International Symposium SP 138 (Edited by A. Nanni and C. W. Dolan), American Concrete Institute, Detroit, MI, 1993, pp. 381-400.
8. Sayed-Ahmed, E. Y., and Shrive, N. G., "A New Steel Anchorage System for Post-Tensioned Applications Using Carbon Fibre Reinforced Plastic Tendons," *Canadian Journal of Civil Engineering,* V. 25, No. 1, 1998, pp. 113-127.
9. Nanni, A., Bakis, C. E., O'Neil, E. F., and Dixon, T. O., "Performance of FRP Tendon-Anchorage Systems for Prestressed Concrete Structures," PCI JOURNAL, V. 41, No. 1, 1996, pp. 34-44.
10. Hodhod, H., and Uomoto, T., " Effect of State of Stress at the Grips and Matrix Properties on Tensile Strength of CFRP Rods," *Proceedings of Japanese Society for Civil Engineering,* V. 17, No. 451, August 1992, pp. 245-252.
11. Shrive, N. G., Sayed-Ahmed, E. Y., Damson, E., Tilleman, and Tadros, G., "Prestressing Anchorage System for Fibre Reinforced Plastic Prestressing Tendons," U.S. Patent Application 08/754186, 1996.
12. Mitsubishi Kasei Corporation, *Leadline Carbon Fibre Tendons/Bars (Product Specifications Manual)*, June 1993, 18 pp.
13. Mitchell, R. A., Woolley, R. M., and Halsey, N., "High Strength End Fittings for FRP Rod and Rope," *Journal of the Engineering Mechanics Division,* V. 100, No. EM4, 1974, pp. 687-706.
14. Grace, Nabil F., and Sayed, George A., "Behaviour of Externally/Internally Prestressed Concrete Composite Bridge System," Proceedings of the Third International Symposium, Japan Concrete Institute, Tokyo, Japan, V. 2, October 1997, pp. 671-678.
15. Campbell, T. I., Keatley, J. P., and Barnes, K. M., "Analysis of an Anchorage for CFRP Prestressing Tendons," Annual Conference of the Canadian Society for Civil Engineering, Halifax, Nova Scotia, Canada, June 1998, pp. 551-560.
16. Al-Mayah, A., "Experimental and Analytical Investigation of Wedge Anchor for CFRP Rod Under Load," MASc Thesis, Department of Civil Engineering, University of Waterloo, Ontario , Canada, 1999, p. 127.
17. Wang, C. T., *Applied Elasticity,* Chapter 4, Plane-Stress and Plane-Strain Problems, McGraw-Hill Inc., New York, NY, 1953.

APPENDIX – NOTATION

u_r, u_s, u_w, u_b = radial displacements of rod, sleeve, wedges, and barrel, respectively
E = modulus of elasticity
E_r, E_s, E_w, E_b = modulus of elasticity of rod, sleeve, wedges, and barrel, respectively
ν_r, ν_s, ν_w, ν_b = Poisson's ratio of rod, sleeve, wedges, and barrel, respectively
p_1 = radial pressure on outer surface of rod and inner surface of sleeve
p_2 = radial pressure on outer surface of sleeve and inner surface of wedges
p_3 = radial pressure on outer face of wedges and inner surface of barrel
p_4 = radial pressure on outer face of barrel
r_{or} = outer radius of rod
r_{is}, r_{os} = inner and outer radius of sleeve
r_{iw}, r_{ow} = inner and outer radius of wedges
r_{ib}, r_{ob} = inner and outer radius of barrel
δ = difference between original outer radius of wedges and matching inner radius of barrel at a specific location